

**Charge radii and ground state structure of lithium isotopes: Experiment and theory reexamined**W. Nörtershäuser,<sup>1,2</sup> T. Neff,<sup>2</sup> R. Sánchez,<sup>3</sup> and I. Sick<sup>4</sup><sup>1</sup>*Institut für Kernchemie, Universität Mainz, D-55099 Mainz, Germany*<sup>2</sup>*GSI Helmholtzzentrum für Schwerionenforschung GmbH, D-64291 Darmstadt, Germany*<sup>3</sup>*Helmholtzinstitut Mainz, Johannes Gutenberg-Universität, D-55099 Mainz, Germany*<sup>4</sup>*Departement für Physik, Universität Basel, CH-4056 Basel, Switzerland*

(Received 4 November 2010; revised manuscript received 16 June 2011; published 10 August 2011)

Changes in the nuclear charge radii of lithium isotopes were determined using a combination of precise isotope shift measurements and theoretical atomic structure calculations. We discuss the choice of the reference isotope for absolute charge radii determinations in the lithium isotopic chain and report a new value for the charge radius of  ${}^6\text{Li}$ , based on the analysis of the world scattering data. A summary of the lithium nuclear charge radii obtained in this way is presented. Additionally, new calculations in fermionic molecular dynamics for the lithium isotopes were performed. We summarize the status of the lithium nuclear charge radii, magnetic dipole and electric quadrupole moments from experimental investigations and compare them to the results of various microscopic and three-body nuclear models.

DOI: [10.1103/PhysRevC.84.024307](https://doi.org/10.1103/PhysRevC.84.024307)

PACS number(s): 21.10.Gv, 21.10.Ft, 21.10.Ky, 21.60.De

**I. INTRODUCTION**

Nuclear ground state properties of stable and short-lived isotopes of the lightest elements are benchmark tests for nuclear structure calculations and have as such attracted much interest for many years. Laser spectroscopy is known to provide accurate and reliable data of nuclear properties [1,2]. Magnetic dipole and electric quadrupole moments were determined for light short-lived isotopes by laser spectroscopy and  $\beta$ -NMR measurements after nuclear polarization by optical pumping and provided important information about the spin and structure of halo nuclei [3–7]. From the isotope shift in an optical transition, the change in the mean square nuclear charge radius can be extracted based on very general assumptions and without the necessity to rely on a particular nuclear model. Hence, this technique is said to be nuclear-model independent. Optical isotope shift measurements were already used for a long time to determine changes in the nuclear charge radii for medium-heavy and heavy short-lived isotopes [1,2,8,9], when it was still not possible to determine nuclear charge radii for short-lived isotopes of the lightest elements. This became feasible only a few years ago, when high-precision atomic structure calculations [10–14] were combined with sensitive and accurate isotope shift measurements [15–21] of the most exotic nuclei in the lower region of the nuclear chart.

While isotope shift measurements in an optical transition are very sensitive to structural changes in the nuclear charge distribution along the isotopic chain and can even be applied for very short-lived species online, they cannot provide absolute charge radii. To calculate rms charge radii  $R_c$  along the isotopic chain, at least one reference radius—usually of a stable isotope—has to be known. Complementary approaches are elastic electron-scattering or muonic-atom spectroscopy [22,23], since they provide absolute nuclear charge radii, but have only limited accuracy and are only applicable to stable isotopes so far.

In recent years it has become possible to perform *ab initio* calculations for light nuclei based on realistic nucleon-nucleon and three-nucleon interactions up to about  $A \approx 12$ . Examples are Green's function Monte Carlo (GFMC) calculations [24,25] and the no-core shell model (NCSM) [26–28]. Very recently a new approach has been presented that solves chiral effective field theory directly on the lattice [29]. *Ab initio* calculations are computationally very expensive and face many challenges, especially for exotic nuclei. The NCSM for example is not very well suited for weakly bound clustered nuclei as the harmonic oscillator basis has the wrong asymptotics.

Other microscopic and nonmicroscopic models have been developed to address the special properties of light nuclei employing effective interactions. Among them are fermionic molecular dynamics (FMD) [30], the stochastic variational multi-cluster model (SVMC) [31], the tensor-optimized shell model (TOSM) [32], and other three-body models (3BM).

This paper consists of three parts. First, we report on the extraction of a consistent set of nuclear charge radii for all lithium isotopes based on the combination of laser-spectroscopic isotope shift measurements reported in [15,16,18,21]. Therefore, the *world* data on elastic electron scattering of  ${}^6\text{Li}$ , performed about 40 years ago [33–35], is analyzed to obtain a reference radius as accurate as possible, including reliable uncertainties. Using this reference radius, a summary of nuclear charge radii of all lithium isotopes is presented.

In the second part we present calculations in the fermionic molecular dynamics (FMD) approach for  ${}^{6-9}\text{Li}$ . We discuss how the evolution of the charge radii reflects the change in the structure from  ${}^6\text{Li}$  and  ${}^7\text{Li}$ , where we find pronounced clustering in the wave function, to  ${}^8\text{Li}$  and  ${}^9\text{Li}$  where the structure is closer to the mean-field picture. Whereas we did not succeed in a consistent description of  ${}^{11}\text{Li}$  in the FMD approach we can still draw some conclusions by analyzing

the  $(p_{1/2})^2$  and  $(s_{1/2})^2$  configurations. In addition we use the FMD calculations to evaluate the spin-orbit contribution to the nuclear charge radius for the different isotopes.

Finally, we compare the measured ground-state properties of the lithium isotopes to the results of FMD and other theoretical approaches. In case of  $^{11}\text{Li}$  the results of three-body models, the stochastic variational multi-cluster model (SVMC) and the tensor-optimized shell model (TOSM) will be discussed. One interesting question here is whether the contributions from the center-of-mass effect and core polarization contributions to the charge radius can be disentangled.

## II. EXPERIMENTAL DETERMINATION OF LITHIUM CHARGE RADII

### A. Extraction of $\delta\langle r_c^2 \rangle$ from isotope shift measurements of lithium isotopes

An extensive description of the experimental technique and details of the mass shift calculations are presented in a previous paper [21] and will not be discussed here. Instead, we will shortly summarize how charge radii of light isotopes are obtained by combining high-accuracy isotope shift measurements and atomic mass shift calculations. The isotope shift

$$\delta\nu_{\text{IS}}^{A,A'} = \nu^{A'} - \nu^A \quad (1)$$

is the difference in transition frequency between two isotopes in an electronic transition. The addition or removal of neutrons causes a change in the nuclear mass [mass shift (MS)] and a change in the nuclear charge distribution [field shift (FS)]

$$\delta\nu_{\text{IS}}^{A,A'} = \delta\nu_{\text{MS}}^{A,A'} + \delta\nu_{\text{FS}}^{A,A'}. \quad (2)$$

The mass shift includes all nuclear mass-dependent terms and can be written as

$$\delta\nu_{\text{MS}}^{A,A'} = K_{\text{MS}} \cdot \frac{M_{A'} - M_A}{M_A M_{A'}}, \quad (3)$$

with the mass-shift constant  $K_{\text{MS}}$ . The field shift can be factorized into an electronic part  $F$  and the change in the mean square nuclear charge radius  $\delta\langle r_c^2 \rangle^{A,A'}$

$$\begin{aligned} \delta\nu_{\text{FS}}^{A,A'} &= F \cdot \delta\langle r_c^2 \rangle^{A,A'} \\ &= \frac{2\pi Z e}{3} \Delta |\Psi(0)|^2 \cdot [R_c^2(A') - R_c^2(A)]. \end{aligned} \quad (4)$$

If the mass shift and the electronic factor  $F$ , determined by the change of the electron probability at the nucleus  $\Delta |\Psi(0)|^2$  in the optical transition, can both be provided by theory with sufficient accuracy, one can easily obtain the change in the mean square nuclear charge radius from an accurate spectroscopic determination of the isotope shift

$$\delta\langle r_c^2 \rangle^{A,A'} = \frac{\delta\nu_{\text{IS,Exp}}^{A,A'} - \delta\nu_{\text{MS,Theory}}^{A,A'}}{F_{\text{Theory}}}. \quad (6)$$

In principle, this *ab initio* approach can be used for all elements. Unfortunately, up to now theory can provide the required accuracy only for two- and three-electron systems in the case of atomic systems with low  $Z$ . This is caused by

the fact that the correlations between all electrons have to be taken into account to obtain high accuracy for the mass shift contribution. But the complicated correlation integrals can be solved only in these few-electron cases. At the same time, the light elements are those, for which the highest accuracy is required to determine the nuclear charge radius, because the field shift is only a  $10^{-4}$  correction to the dominant mass shift. In lithium for example, the field shift factor  $F$  is about  $1.5 \text{ MHz/fm}^2$ , i.e., the field shift is of the order of 1 MHz while the mass shift between neighboring isotopes is of the order of 10 000 MHz. However, atomic theory has now developed the required tools to calculate the mass shift to an accuracy of about 10 kHz and better [12,13,21]. In parallel, new experimental techniques were developed to measure isotope shifts of the lightest elements with accuracies of 100 kHz and better.

The values for the nuclear charge radii of the lithium isotopes have been slightly changing since the first publication on charge radii measurements on lithium isotopes in 2004 [15]. This has led to some confusion about the most reliable set of charge radii and was even misinterpreted as a model dependence of the technique [36]. We want to stress that, apart from a small contribution of nuclear polarizability correction, the extraction of the change in the mean square nuclear charge radius is model independent. The main reasons for varying  $\delta\langle r_c^2 \rangle$  values are an improved accuracy in the atomic structure calculations, improved mass measurements, and, lately, a discussion about the most appropriate reference charge radius. These issues will be shortly addressed in the following sections.

### B. The history of high-precision mass-shift calculations in lithium

Mass-shift calculations for lithium isotopes were continuously improved since the first high-accuracy calculations by Yan and Drake in 2000 [10]. The published values during the last decade are summarized in Table I and plotted in Fig. 1. To demonstrate the influence of the improvements on  $R_c$ , we have also listed the change in the nuclear charge radius of  $^{11}\text{Li}$  relative to  $^6\text{Li}$  according to

$$\Delta R_c^{(6,11)} = \sqrt{R_c^2(^6\text{Li}) + \delta\langle r_c^2 \rangle^{6,11}} - R_c(^6\text{Li}) \quad (7)$$

using  $R_c(^6\text{Li}) = 2.59 \text{ fm}$  (see Sec. II C), the experimental isotope shift  $\delta\nu_{\text{IS,Exp}}^{6,11} = 36555.176(108) \text{ MHz}$  [21] and the electronic factor  $F = 1.570 \text{ MHz/fm}^2$  [37].

While the accuracy of the mass-shift calculations was stepwise increased, as can be seen from the reduction of the estimated uncertainty, there are a few jumps of the calculated value that are clearly larger than the assigned error bar. Firstly, the  $^{11}\text{Li}$  mass value changed considerably by improved experiments and therefore the calculated mass shift changed accordingly: The first direct mass measurement at MISTRAL [40,41] yielded a two-neutron binding energy  $S_{2n}$  of 378(5) keV, more than  $3\sigma$  larger than the previously used value of 300(20) keV from the Atomic Mass Evaluation (AME) in 1995 and 2003 [38,43]. The MISTRAL value was later confirmed and improved in accuracy to  $S_{2n} =$

TABLE I. Accuracy and corrections of the lithium isotopic mass shift calculations.  $\delta\nu_{\text{MS,Theory}}^{6,11}$  are the published values for the mass-dependent part of the isotope shift between  $^{11}\text{Li}$  and  $^6\text{Li}$ . The  $^{11}\text{Li}$  masses used in the respective isotope shift calculations are listed as well as the influence on the change of the charge radius  $\Delta R_c^{(6,11)}$  between  $^6\text{Li}$  and  $^{11}\text{Li}$  according to Eq. (7) using  $R_c = 2.59$  fm for  $^6\text{Li}$ , the experimental isotope shift  $\delta\nu_{\text{IS,Exp}}^{6,11} = 36555.176(108)$  MHz [21] and the electronic factor  $F = 1.570$  MHz/fm<sup>2</sup> [37].

Year	Ref.	$\delta\nu_{\text{MS,Theory}}^{6,11}$ (MHz)	$^{11}\text{Li}$ mass (amu)	$\Delta R_c^{6,11}$ (fm)
2000	Yan & Drake [10]	36 555.34(21)	11.043798(21) [38]	+0.020
2002	Yan & Drake [39]	36 555.11(21)	11.043798(21) [38]	-0.008
2006	Sánchez <i>et al.</i> [18]	36 554.82(18)	11.043714(5) [40]	-0.044
2006	Puchalski <i>et al.</i> [12]	36 554.295(30)	11.043714(5) [40]	-0.111
2008	Yan <i>et al.</i> [13]	36 554.291(24)	11.043714(5) [40]	-0.111
2008	Puchalski & Pachucki [37]	36 554.323(11)	11.04372361(69) [42]	-0.107
2010	Nörtershäuser <i>et al.</i> [21]	36 554.324(9)	11.04372361(69) [42]	-0.107

369.15(65) keV at the TITAN facility at TRIUMF [42]. Compared to the result obtained with the AME value in [10,39], the new measurements cause a change in the charge radius of  $^{11}\text{Li}$  by as much as 0.04 fm [18], which is about 2% of the total charge radius.

In addition, Puchalski and Pachucki [12] improved the calculations of Yan and Drake by identifying a strong cancellation between reduced mass, mass polarization, and the direct electron-nucleus Breit interaction in the relativistic recoil correction. Their value for the relativistic recoil corrections turned out to be more than ten times smaller than the previous value, resulting in a correction of about -380 kHz in the mass shift and a reduced uncertainty. A numerical instability in the previous calculations by Yan and Drake was the reason for this discrepancy and soon corrected by the authors [13].

Finally, measurements at RIKEN determined a strong low-lying dipole strength [44] of the  $^{11}\text{Li}$  nucleus. Puchalski and Pachucki [12] pointed out that this has some influence on the isotopic shift due to the associated nuclear polarizability that makes the nucleus sensitive to the electric field of the electrons. This, in turn, leads to a shift of the electron energies that is not negligible at the level of accuracy of the atomic calculations. However, the total amount of the polarizability

shift is only 35(8) kHz, which is four times smaller than the experimental uncertainty in the isotope shift measurement and corresponds to a change in the nuclear charge radius of  $^{11}\text{Li}$  by only 0.007 fm.

Since 2008, the calculations of the two groups are in accordance with each other within the estimated uncertainty and could even be further improved [21]. Now, agreement on the 1 kHz level (relative uncertainty  $3 \times 10^{-7}$ ) is demonstrated, which is two orders of magnitude more accurate than the experimentally determined isotope shift.

### C. Reference radii of stable lithium isotopes

If the charge radius of at least one reference isotope  $A$  is known, absolute nuclear charge radii for all isotopes  $A'$  of the isotopic chain can be determined from the isotope shift investigations according to

$$R_c(^{A'}\text{Li}) = \sqrt{R_c^2(^A\text{Li}) + \delta \langle r_c^2 \rangle^{A,A'}}. \quad (8)$$

Elastic electron-scattering is known to provide reliable nuclear charge radii of stable isotopes. In previous publications on the lithium isotopes [15,16,18], a value of  $R_c(^7\text{Li}) = \sqrt{\langle r_c^2 \rangle_7} = 2.39(3)$  fm was used as reference radius. This value is the weighted average of elastic electron scattering from [33,34].

In this publication, we use the radius of  $^6\text{Li}$  as absolute reference for the following reasons: For  $^6\text{Li}$ , additional precise data in the region of maximal sensitivity to the rms-radius are available [35] and elastic scattering could be very well separated from inelastic scattering. In  $^7\text{Li}$ , the first excited state at 0.478 MeV could not be resolved in the experiments [33,34]. Moreover, the contribution of C2 scattering from the quadrupole distribution, which could not be separated, is negligible for  $^6\text{Li}$  while it makes a significant contribution for  $^7\text{Li}$ , and its subtraction would introduce substantial uncertainties.

In order to obtain the most accurate radius, we have performed a new analysis of the *world* data [33–35] for  $^6\text{Li}$ . The cross sections, which were initially measured relative to the then available data for scattering from the proton or carbon [45,46], were renormalized to state-of-the-art fits to the *world* data [47,48]. A phase-shift code was used to account for the Coulomb distortion.

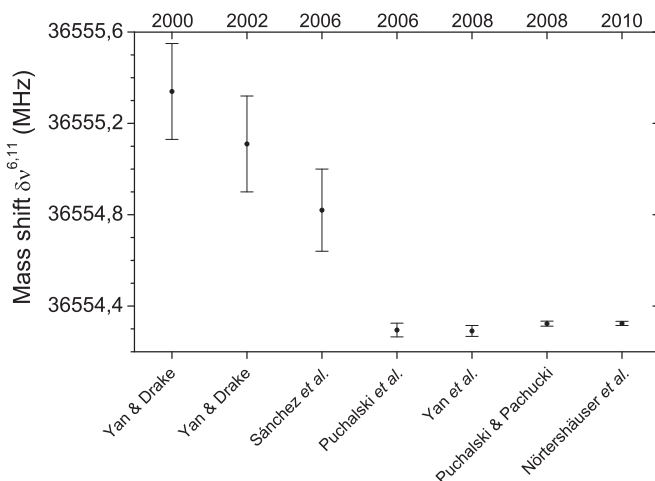


FIG. 1. Calculated mass shifts between  $^6\text{Li}$  and  $^{11}\text{Li}$  during the last decade. See Table I for references.

We have performed two types of analyses. First, one of the standard parametrizations of the charge density for  ${}^6\text{Li}$  was used [33,35]. This parametrization allows for a good fit of the data. The resulting radius has a model dependence that is difficult to quantify. In particular, the effect of the large-radius tail of the charge density is rather uncertain, which is important due to the low deuteron and proton separation energy.

In the second, more trustworthy, analysis we parametrized the interior part of the charge density using the “model-independent” approach of [48]. The *shape* of the density at large radii was taken from the Green’s function Monte Carlo (GFMC) calculation of [49]. This calculation reproduces accurately the  ${}^6\text{Li}$  binding energy and thus has a density at large  $r$  that has the correct shape. In a single-particle model the large- $r$  density would be proportional to a Whittaker function  $W_{-\eta, 1/2}^2(2\kappa r)/r^2$ . For  ${}^6\text{Li}$ , such a single-particle picture would be too simpleminded, however, given the (partial)  $\alpha$ - $d$  cluster structure, which would lead to a different large- $r$  behavior. The GFMC calculation, which corresponds to an exact solution of the Schrödinger equation for a realistic nucleon-nucleon potential, automatically accounts for the various wave function components and does not require *a priori* assumptions on the single particle/cluster nature.

To obtain the large- $r$  (relative) charge density, the GFMC point density [50] was folded with the intrinsic proton and neutron charge densities. From GFMC, we thus obtained the (relative) charge density at radii  $r \geq 2.8$  fm, where the density has fallen to less than 4% of its central value. The density, parametrized using the sum-of-Gaussians (SOG) approach, was fitted to the  $(e, e)$  cross sections and the (relative) large- $r$  GFMC density. The statistical uncertainty of the resulting radius was obtained from the error matrix, while the systematic one was obtained by changing the data by their quoted systematic uncertainty, refitting, and by adding quadratically the resulting changes.

When fitting the data up to a momentum transfer of  $q = 2.4 \text{ fm}^{-1}$  (where the quadrupole form factor still contributes negligibly) we find a  $\chi^2$  of 113 for 90 degrees of freedom. The ratio of the experimental and fitted cross sections are shown in Fig. 2 for the parametrization with the relative charge density at  $r \geq 2.8$  fm given by GFMC calculations. The resulting rms radius is

$$R_c({}^6\text{Li}) = 2.589 \pm 0.039 \text{ fm}, \quad (9)$$

where the uncertainty covers both the statistical and systematic uncertainties. The radius is slightly larger than the most reliable previous value [35] of 2.56(5) fm, because the model densities used in [33,35] had a too steep (Gaussian) fall-off at very large  $r$ .

The uncertainty we obtain for the  ${}^6\text{Li}$  radius is somewhat larger than the one previously quoted for  ${}^6\text{Li}$  or  ${}^7\text{Li}$ , obtained by averaging published values from individual experiments. This is a consequence of the fact that the present radius is not dependent on specific models used to parametrize the densities, and the fact that we do account in a rather conservative fashion for the systematic errors (normalization errors) of the individual data sets.

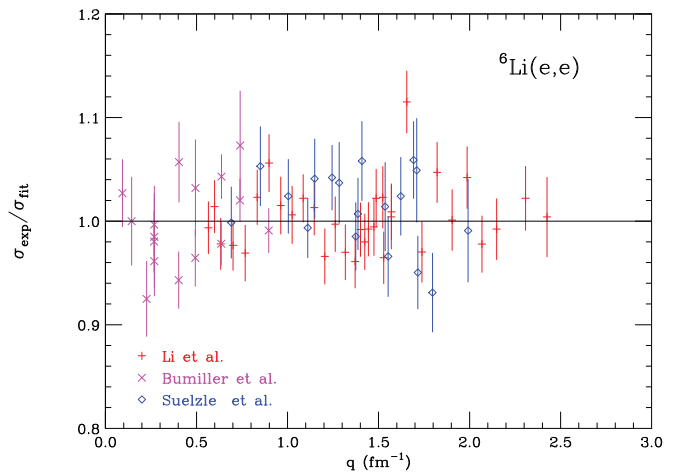


FIG. 2. (Color online) Ratio of experimental and fit cross sections for the parametrization with the relative charge density at  $r \geq 2.8$  fm given by Green’s function Monte Carlo (GFMC) calculations (see text).

#### D. Nuclear charge radii of unstable lithium isotopes

The measured isotope shifts reported in [21] can now be combined with the mass-shift calculations using Eq. (6) to calculate  $\delta\langle r_c^2 \rangle$  and with the absolute charge radius of  ${}^6\text{Li}$  to obtain charge radii  $R_c$  for all lithium isotopes according to Eq. (8). Results are summarized in Table II and discussed below together with nuclear model predictions. Please note that the isotope shifts reported in [21] were slightly changed compared to the first report in [18] because of an additional small correction for the differential second-order Doppler shift and a reanalysis of all systematic uncertainties.

### III. FERMIONIC MOLECULAR DYNAMICS CALCULATIONS FOR THE LITHIUM ISOTOPES

To obtain a better understanding of the physics behind the evolution of the charge radii along the isotope chain we performed calculations using the fermionic molecular dynamics (FMD) approach. FMD allows to consistently describe nuclei with a mean-field dominated structure and nuclei featuring cluster and halo structures. The FMD wave functions will also allow us to explicitly evaluate the spin-orbit contribution to the charge radii.

FMD has been used successfully for light nuclei in the  $p$  and  $sd$  shells. It was used for example to study the structure of the Hoyle state in  ${}^{12}\text{C}$  [51], the properties of the beryllium isotopes [52] and to explain the evolution of the charge radii in neon isotopes [53]. Recently a calculation of the radiative capture reaction  ${}^3\text{He}(\alpha, \gamma){}^7\text{Be}$  with a consistent description of bound and scattering states [54] was achieved. A general discussion of the FMD approach is given in [30].

#### A. Fermionic molecular dynamics

FMD uses intrinsic many-body basis states that are Slater determinants

$$|Q\rangle = A\{|q_1\rangle \otimes \dots \otimes |q_A\rangle\} \quad (10)$$

TABLE II. Experimental isotope shifts  $\delta\nu_{\text{IS,Exp.}}$ , calculated mass shifts  $\delta\nu_{\text{MS,Theory}}$ , extracted field shift contributions  $\delta\nu_{\text{FS}}$ , field shift coefficient  $F$ , and changes in the mean square nuclear charge radii  $\delta\langle r_c^2 \rangle^{6,A}$ . All shifts are given relative to  ${}^6\text{Li}$  and values are taken from [21]. Absolute charge radii  $R_c$  are calculated using Eq. (8) and the charge radius of  ${}^6\text{Li}$  obtained from our analysis of the world scattering data.

${}^A\text{Li}$	$\delta\nu_{\text{IS,Exp.}}$ (MHz)	$\delta\nu_{\text{MS,Theory}}$ (MHz)	$\delta\nu_{\text{FS}}$ (MHz)	$F$ (MHz/fm <sup>2</sup> )	$\delta\langle r_c^2 \rangle^{6,A}$ (fm <sup>2</sup> )	$R_c$ (fm)
${}^6\text{Li}$	0.0	0.0	0.0	0.0	0.0	2.589(39)
${}^7\text{Li}$	11 453.970(34)	11 452.821(3)	1.149(34)	-1.5719(16)	-0.731(22)	2.444(42)
${}^8\text{Li}$	20 089.735(50)	20 087.802(5)	1.933(51)	-1.5719(16)	-1.230(32)	2.339(44)
${}^9\text{Li}$	26 787.236(50)	26 784.621(7)	2.615(50)	-1.5720(16)	-1.663(32)	2.245(46)
${}^{11}\text{Li}$	36 555.176(108)	36 554.324(9)	0.852(108)	-1.5703(16)	-0.543(69)	2.482(43)

built using Gaussian wave packets as single-particle states

$$\langle \vec{x} | q_k \rangle = \exp \left\{ -\frac{(\vec{x} - \vec{b}_k)^2}{2a_k} \right\} \otimes | \chi_k^\uparrow, \chi_k^\downarrow \rangle \otimes | \xi \rangle. \quad (11)$$

The parameters of the wave packets are the widths  $a_k$  and the complex vectors  $\vec{b}_k$  that encode the mean positions and mean momenta of the wave packets. The spin of the wave packets can take any direction, the isospin  $\pm 1$  corresponds to either protons or neutrons. The wave-packet basis is very flexible—it contains the harmonic oscillator shell model states and Brink-type cluster states as special limiting cases. The width parameters  $a_k$  are also variational parameters and can be different for each wave packet. This is especially useful for the description of spatially extended halo states.

The intrinsic states  $|Q\rangle$  reflect deformation or clustering and break the symmetries of the Hamiltonian with respect to parity, rotation and translation. To restore the symmetries the intrinsic basis states are projected on parity, angular momentum and total linear momentum

$$|Q; J^\pi MK; \vec{P} = 0\rangle = P^\pi P_{MK}^J P^{\vec{P}=0} |Q\rangle. \quad (12)$$

In a full FMD calculation the many-body Hilbert space is spanned by a set of  $N$  intrinsic basis states  $\{|Q^{(a)}\rangle, a = 1, \dots, N\}$ . For light nuclei like the lithium isotopes the basis states are obtained by variation after parity and angular momentum projection. Additional basis states can be obtained by constraints on the intrinsic wave function. In the end the full many-body state is obtained by diagonalizing the Hamiltonian in the set of nonorthogonal basis states  $\{|Q^{(a)}\rangle\}$ .

### B. Effective interaction

The FMD basis is well suited to describe long-range correlations but it is not possible to describe explicitly short-range correlations as induced by realistic interactions. Therefore an effective interaction for the FMD model space is needed. Starting from the realistic Argonne V18 interaction we use the unitary correlation operator method (UCOM) to explicitly include short-range central and tensor correlations [55–57]. The resulting UCOM interaction is a low-momentum interaction where the bulk of the tensor force has been transformed into the central force. There is a remaining long-range part of the tensor force.

First successful *ab initio* type calculations using FMD wave functions and the UCOM interaction have been performed for the  ${}^3\text{He}(\alpha, \gamma){}^7\text{Be}$  and  ${}^3\text{H}(\alpha, \gamma){}^7\text{Li}$  reactions [54]. Although the properties of the  ${}^7\text{Be}$  and  ${}^7\text{Li}$  ground states are reproduced fairly well, the splitting between the  $3/2^-$  and  $1/2^-$  bound states is too small when compared to experiment. This indicates that the spin-orbit strength is too small. In an *ab initio* picture additional spin-orbit strength will come from three-body forces. In this paper, as in previous structure studies, we choose to employ a phenomenological two-body correction term that contains a central momentum-dependent part and an additional spin-orbit part to make up for missing three-body forces. The parameters of the correction term are fitted to binding energies and radii of double-closed shell nuclei.

In this paper we use a slightly weaker spin-orbit correction term than in previous structure studies. This improves the description of the spectra of the lithium isotopes and also provides better results for the electromagnetic properties. On the other hand the binding energies are now somewhat smaller and slightly underestimate the experimental binding energies.

### C. FMD results for ${}^6\text{--}9\text{Li}$

In the present paper we generate the many-body basis states by variation after projection (VAP) on parity and angular momentum. For each isotope the variation is performed for the spins of the three lowest-lying states. In Fig. 3 we show cuts through the proton- and neutron-densities of the intrinsic states obtained for the ground state spin. The density distributions already reflect the  ${}^4\text{He}$  plus deuteron and  ${}^4\text{He}$  plus triton cluster structure in  ${}^6\text{Li}$  and  ${}^7\text{Li}$ , respectively. For the heavier isotopes  ${}^8\text{Li}$  and  ${}^9\text{Li}$  a more mean-field-like picture emerges. This is not surprising as we have low cluster thresholds in  ${}^6\text{Li}$  and  ${}^7\text{Li}$  that are much lower than the proton or neutron thresholds. In  ${}^8\text{Li}$  and  ${}^9\text{Li}$  on the other hand the neutron separation thresholds are much lower than multicenter thresholds. The general trend of decreasing charge radii can already be deduced from these intrinsic proton distributions.

For the full calculation we generate additional basis states by constraining the matter radius of the intrinsic states during the minimization. For each spin we constrain to five or six different radii, we therefore have 15–18 intrinsic basis states for each isotope. In  ${}^6\text{Li}$  and  ${}^7\text{Li}$  the intrinsic states react to the radius constraint essentially by a smaller or larger separation

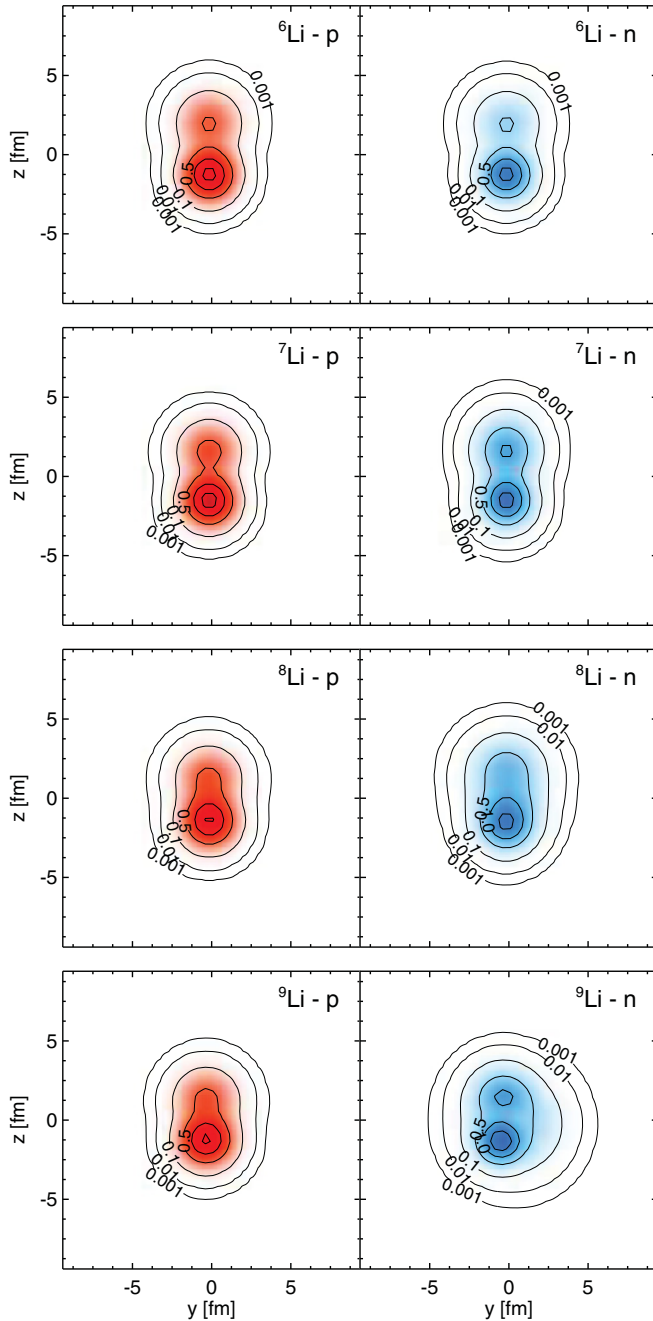


FIG. 3. (Color online) Cuts through the intrinsic densities of FMD configurations of  ${}^6\text{--}9\text{Li}$  obtained in variation after projection (VAP) on the ground state spin. Proton densities on the left, neutron densities on the right. Contour lines are in units of half nuclear matter density.

of the clusters. In  ${}^8\text{Li}$  and  ${}^9\text{Li}$  the constraint mostly affects the neutron distributions.

The gain in binding energy comparing the full multiconfiguration mixing calculation with the result from a single configuration is between 2 and 3 MeV for all isotopes. For the charge radii the effect decreases significantly from  ${}^6\text{Li}$  and  ${}^7\text{Li}$ , where the charge radii are larger by 0.18 fm and 0.17 fm respectively, to  ${}^9\text{Li}$ , where the charge radius in the multiconfiguration mixing calculation is larger by only

0.05 fm. This reflects the softness of the energy surface in  ${}^6\text{Li}$  and  ${}^7\text{Li}$  with respect to the cluster separation.

Results for binding energies, charge radii, magnetic and electric quadrupole moments of the ground states are summarized in Sec. IV A. The binding energies are slightly too small compared to experiment but follow the experimental trend. The quadrupole moment of  ${}^6\text{Li}$  is very sensitive to details of the calculation. It becomes positive when the tensor terms of the interaction are not included although the binding energy is almost unchanged. Also the quadrupole moment of  ${}^8\text{Li}$  becomes significantly smaller when the tensor terms in the interaction are omitted. Furthermore the level ordering for some low-lying excited states in  ${}^8\text{Li}$  and  ${}^9\text{Li}$  becomes wrong when the tensor force is not included.

Overall the FMD results give a very reasonable description of the electromagnetic properties of the nuclei  ${}^6\text{--}9\text{Li}$ . The charge radii of  ${}^7\text{Li}$  and especially  ${}^6\text{Li}$  turn out to be somewhat too small compared to experiment. This could be improved by adding explicit deuteron and triton cluster configurations to better describe the tail of the wave functions as has been done in [54].

#### D. FMD results for ${}^{11}\text{Li}$

${}^{11}\text{Li}$  is a very peculiar nucleus. It is a so-called Borromean nucleus as both  ${}^{10}\text{Li}$  and the dineutron are unbound. The two-neutron separation energy is only 369 keV which makes  ${}^{11}\text{Li}$  one of the prime candidates for three-body cluster models. In a microscopic model a nucleus like  ${}^{11}\text{Li}$  is extremely difficult to describe. We did not succeed yet in a consistent calculation within the FMD approach. Nevertheless we can draw some conclusions regarding its structure from first results.

From three-body models we know that there are two main configurations in the  ${}^{11}\text{Li}$  ground state—a  ${}^9\text{Li}$  core plus two neutrons in  $(p_{1/2})^2$  or  $(s_{1/2})^2$  configurations. By variation after projection for  ${}^{11}\text{Li}$  on the ground state spin  $3/2^-$  we easily obtain an intrinsic configuration that corresponds mainly to a  $(p_{1/2})^2$  configuration. These  $p$  orbits are however not simple harmonic oscillator orbits but have a more extended tail reflecting the very weak binding. The neutron density distribution as shown in the upper part of Fig. 4 therefore extends further out than in  ${}^9\text{Li}$ . A second local minimum in the energy surface can be found for an  $(s_{1/2})^2$  configuration as is shown in the lower part of Fig. 4. Here we find an intrinsic state that is very similar to  ${}^9\text{Li}$  obtained in variation after projection plus two neutrons in very extended  $s$  orbits. It is interesting to note that in case of the  $(s_{1/2})^2$  configuration the effect of the center-of-mass projection is very large—3.6 MeV versus only 0.7 MeV for the  $(p_{1/2})^2$  configuration. For the  $(s_{1/2})^2$  configuration we therefore perform the variation after parity, angular momentum and total linear momentum projection. In all other cases the linear momentum projection is only performed after the variation.

We compare the results for the two  ${}^{11}\text{Li}$  configurations and for a single  ${}^9\text{Li}$  configuration in Table III. There are some interesting observations to be made: The binding energy of the  $(p_{1/2})^2$  configuration with respect to the single  ${}^9\text{Li}$  configuration is about 1 MeV, much larger than the experimental

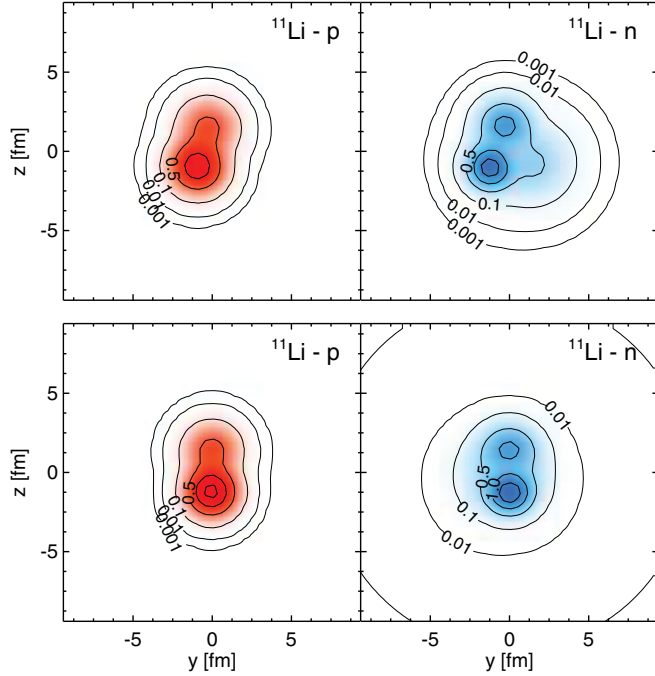


FIG. 4. (Color online) Cuts through intrinsic densities of FMD configurations obtained in variation after projection for  $^{11}\text{Li}$  in  $(p_{1/2})^2$  (top) and  $(s_{1/2})^2$  (bottom) configurations.

value. This value should be reduced significantly in a more extended calculation. In  $^9\text{Li}$  we gain about 2 MeV in binding energy by multiconfiguration mixing. We expect that in the  $(p_{1/2})^2$  configuration of  $^{11}\text{Li}$  the effect will be smaller as we are dealing with a closed shell configuration for the neutrons. The single  $(s_{1/2})^2$  configuration is actually unbound with respect to the  $^9\text{Li}$  core and the binding energy is significantly smaller than for the  $(p_{1/2})^2$  configuration. In a full calculation we expect two effects which should provide more binding. (1) Within the core plus two neutron picture we should gain about 2 MeV by going from the single configuration for the  $^9\text{Li}$  core to the corresponding multiconfiguration mixing result. (2) In addition a better description of the halo neutrons by going beyond a single configuration should further lower the energy. Under these assumptions we expect the energies of the  $(p_{1/2})^2$  and  $(s_{1/2})^2$  configurations to be pretty similar. In this case of two configurations with almost degenerate energies significant mixing will occur even if the mixing matrix element between the two configurations is small. With the present wave functions the mixing between the  $(p_{1/2})^2$  and  $(s_{1/2})^2$  configurations is indeed very weak. The mixing between the configurations could also be enhanced via a third configuration of  $(d_{5/2})^2$  nature or configurations with core polarization.

For our understanding of the electromagnetic observables it is also interesting to see how these observables change in the different  $^{11}\text{Li}$  configurations when compared to the  $^9\text{Li}$  results. We observe an increase in the charge radius for the  $(p_{1/2})^2$  configuration from 2.22 fm to 2.31 fm and for the  $(s_{1/2})^2$  configuration to 2.46 fm. We also observe sizable increases in the magnetic and quadrupole moments for the  $(p_{1/2})^2$  configurations, whereas they are almost unchanged for the  $(s_{1/2})^2$  configuration. If we further investigate our

TABLE III. Observables for the FMD  $(p_{1/2})^2$  and  $(s_{1/2})^2$  configurations in  $^{11}\text{Li}$  obtained by variation after projection on the ground state spin compared with the results for a single  $^9\text{Li}$  configuration obtained by variation after projection.

	$^9\text{Li}$	$^{11}\text{Li} - (p_{1/2})^2$	$^{11}\text{Li} - (s_{1/2})^2$
$E_B$ (MeV)	41.89	42.87	41.44
$R_c$ (fm)	2.22	2.31	2.46
$\mu$ ( $\mu_N$ )	3.33	3.66	3.36
$Q_s$ (mb)	-26.7	-28.7	-26.3

wave functions we find that the proton radius with respect to the center-of-charge increases in the  $(p_{1/2})^2$  configuration but is unchanged in the  $(s_{1/2})^2$  configuration. This indicates a certain degree of core polarization in the  $(p_{1/2})^2$  configuration. A quantification of the core polarization would however require the calculation of two-nucleon overlap functions or spectroscopic factors which is not yet implemented in the FMD code.

#### IV. COMPARISON OF GROUND-STATE PROPERTIES IN EXPERIMENT AND THEORY

For comparison of the experimental values with theory, we have to consider that theoretical approaches treat protons and neutrons as point-like particles. Charge radii reported by such models must be converted from mean square (ms) point-proton radii  $\langle r_{pp}^2 \rangle$  into ms nuclear charge radii  $R_c^2 = \langle r_c^2 \rangle$ . The latter can be expressed by  $\langle r_{pp}^2 \rangle$ , taking into account the finite size of the nucleons by folding in the proton ms charge radius,  $R_p^2 = 0.769(12) \text{ fm}^2$  [58], and the neutron ms charge radius  $R_n^2 = -0.117(4) \text{ fm}^2$  [59], according to

$$\langle r_c^2 \rangle = \langle r_{pp}^2 \rangle + R_p^2 + \frac{N}{Z} R_n^2 + \frac{3\hbar^2}{4M_p^2 c^2} + \langle r_c^2 \rangle_{so}. \quad (13)$$

The term  $3\hbar^2/4M_p^2 c^2 \sim 0.033 \text{ fm}^2$  is the Darwin-Foldy correction [60] which takes into account the ‘‘Zitterbewegung’’ of the proton with mass  $M_p$ . In addition to [60], the last term  $\langle r_c^2 \rangle_{so}$  has been included which is the spin-orbit charge density introduced in [61]. The contribution of this term in the case of the lithium nuclei has been discussed in [62,63]. We write the spin-orbit contribution as

$$\langle r_c^2 \rangle_{so} = \frac{1}{Z} \sum_i \langle r_c^{2(i)} \rangle_{so} = \frac{2}{Z} \sum_i \frac{\hbar^2 \mu_i}{M^2 c^2} \langle \vec{l} \cdot \vec{s} \rangle_i, \quad (14)$$

where  $i$  runs over all nucleons and  $\mu_i$  are the anomalous magnetic moments of the neutron ( $\mu_n = -1.91$ ) and the proton ( $\mu_p = 2.79 - 1 = 1.79$ ),  $M$  is the nucleon mass. The expectation value of the spin-orbit operator in a single particle state where orbital angular momentum  $\vec{l}$  and spin  $\vec{s}$  are coupled to total angular momentum  $\vec{j}$  is

$$\langle \vec{l} \cdot \vec{s} \rangle = \begin{cases} -\frac{1}{2}(l+1); & j = l - \frac{1}{2} \\ \frac{1}{2}l; & j = l + \frac{1}{2} \end{cases}. \quad (15)$$

TABLE IV. Proton and neutron spin-orbit contributions to the nuclear charge radii  $\langle r_c^2 \rangle_{so}$  for  ${}^6\text{--}9\text{Li}$  obtained using full FMD wave functions. Values are also given for single  $(p_{1/2})^2$  and  $(s_{1/2})^2$   ${}^{11}\text{Li}$  configurations and a corresponding  ${}^9\text{Li}$  configuration (VAP). Values for the configuration-mixed wave functions according to the tensor-optimized shell model (TOSM) [67,68] and a three-body model (3BM) [36] are included for  ${}^9,{}^{11}\text{Li}$  (see text).

Isotope	Model	$\langle r_c^2 \rangle_{so}^p$ (fm <sup>2</sup> )	$\langle r_c^2 \rangle_{so}^n$ (fm <sup>2</sup> )
${}^6\text{Li}$	FMD	+0.006	-0.006
${}^7\text{Li}$	FMD	+0.012	-0.020
${}^8\text{Li}$	FMD	+0.011	-0.056
${}^9\text{Li}$	FMD	+0.021	-0.084
${}^9\text{Li}$	FMD (VAP)	+0.023	-0.089
${}^{11}\text{Li} - (p_{1/2})^2$	FMD (VAP)	+0.024	-0.003
${}^{11}\text{Li} - (s_{1/2})^2$	FMD (VAP)	+0.023	-0.088
${}^9\text{Li}$ (free)	TOSM <sup>a</sup>	+0.026	-0.091
${}^9\text{Li}$ in ${}^{11}\text{Li}$	TOSM <sup>b</sup>	+0.026	-0.097
$2n$ halo in ${}^{11}\text{Li}$	TOSM <sup>c</sup>		+0.052
${}^{11}\text{Li}$	TOSM <sup>d</sup>	+0.026	-0.045
$2n$ halo in ${}^{11}\text{Li}$	3BM <sup>e</sup>		+0.048

<sup>a</sup>Wave function according to [69]: 84.4%  $0p\text{-}0h$ , 8.7%  $2p\text{-}2h$   $(1s)_{10}^{-2}(1p_{1/2})_{10}^2$  ( $T = 0, n - p$ ), 6.8%  $2p\text{-}2h$   $(1p_{3/2})_{01}^{-2}(1p_{1/2})_{01}^2$  ( $T = 1, n - n$ ).

<sup>b</sup>Wave function according to [69]: 89%  $0p\text{-}0h$ , 4.9%  $2p\text{-}2h$   $(1s)_{10}^{-2}(1p_{1/2})_{10}^2$  ( $T = 0, n - p$ ), 5.9%  $2p\text{-}2h$   $(1p_{3/2})_{01}^{-2}(1p_{1/2})_{01}^2$  ( $T = 1, n - n$ ).

<sup>c</sup>Wave function of the halo neutrons according to Table IV (TOSM) in Ref. [68].

<sup>d</sup>Sum of footnotes b and c.

<sup>e</sup>Wave function of the halo neutrons according to Table 4 in [36]:  $(2s_{1/2})^2 \approx 37\%$ ,  $(1p_{1/2})^2 \approx 47\%$ ,  $(1p_{3/2})^2 \approx 9\%$ , and  $J_{\text{halo}} > 0 \approx 7\%$ .

Hence, each  $p_{3/2}$  neutron contributes with  $-0.028$  fm<sup>2</sup>, a  $p_{1/2}$  neutron with  $0.056$  fm<sup>2</sup>, and a  $p_{3/2}$  proton has a spin-orbit contribution of  $0.026$  fm<sup>2</sup>. The spin-orbit term for a specific shell-model configuration can therefore easily be calculated. In the extreme case of a pure  $\pi p_{3/2} \nu p_{3/2}^4$  configuration for  ${}^9\text{Li}$ , this would give a total spin-orbit contribution of  $-0.086$  fm<sup>2</sup>. However,  $jj$  coupling is usually not a particularly good assumption for light nuclei, and  $LS$  or intermediate coupling is often the better choice. Moreover, configuration mixing becomes important, particularly for the nuclei far away from stability, and can have relatively large effects on the spin-orbit term. We have calculated the spin-orbit contribution for the nuclei  ${}^6\text{--}9\text{Li}$  using the FMD wave functions. The contributions from protons and neutrons are listed separately in Table IV. The FMD values for  ${}^6\text{Li}$  are much smaller than expected for a proton or neutron in a  $p_{3/2}$  orbit in the single-particle picture, reflecting the cluster structure of this nucleus. The  $jj$ -coupling picture becomes more accurate for the heavier isotopes but even in  ${}^9\text{Li}$  the spin-orbit contributions deviate significantly from the  $jj$ -coupling estimate. The overall contribution to the charge radii is very small, as proton and neutron contributions largely cancel each other—in  ${}^6\text{Li}$  it is almost zero and becomes largest in  ${}^9\text{Li}$  where the charge radius will change by  $-0.014$  fm due to the spin-orbit contributions. There is an interesting effect in  ${}^{11}\text{Li}$  where the change of the charge

radii due to the spin-orbit contributions will be  $+0.005$  fm and  $-0.014$  fm for the  $(p_{1/2})^2$  and  $(s_{1/2})^2$  configurations, respectively.

Overall, the spin-orbit contribution has a magnitude  $\lesssim 0.08$  fm<sup>2</sup>, which is similar to the size of the uncertainty in the  $R_p^2$  term, raised by the recent Lamb shift measurement in muonic hydrogen [64] that provided a value which is  $0.096$  fm<sup>2</sup> smaller than that obtained from the latest reanalysis of electron-scattering experiments [65,66] and still  $0.060$  fm<sup>2</sup> smaller than the current CODATA value [58]. Since the spin-orbit contribution to the charge radius is strongly model dependent and rather small in size it is neglected when using Eq. (13) to convert point proton radii results of nuclear-structure calculations into nuclear charge radii. However, the spin-orbit contribution to the charge radius was considered to become particularly important in the case of the halo nucleus  ${}^{11}\text{Li}$  [62,63] and this is therefore discussed in more detail in Sec. IV B.

#### A. Summary of nuclear ground state properties of lithium isotopes

Table V summarizes the electromagnetic properties of the ground states of the lithium isotopes from experiment and various nuclear models, including the new results from FMD.

The charge radii are plotted in Fig. 5. Full circles represent the experimental nuclear charge radii with error bars based solely on the uncertainty in the isotope shift measurement and the (negligible) uncertainty in the mass-shift calculations. The gray band along the isotope chain represents the correlated uncertainty including the one estimated for the charge radius of the reference isotope  ${}^6\text{Li}$ .

The FMD calculations as presented in Sec. III reproduce the evolution of the charge radii from  ${}^6\text{--}9\text{Li}$  quite well. The radii for  ${}^6,{}^7\text{Li}$  are slightly underestimated—the inclusion of explicit cluster configurations to the model space, as done in [54], would help in improving the tails of the wave functions. Within the enlarged model space and employing a slightly different interaction a charge radius of  $2.46$  fm was obtained for  ${}^7\text{Li}$ .

The magnetic dipole and electric quadrupole moments agree well with the experimental values for  ${}^6\text{--}9\text{Li}$  (Fig. 6) and confirm the picture we have developed for the structure of the lithium isotopes. Comparing the experimental results for  ${}^{11}\text{Li}$  with the discussion based on single FMD configurations in Sec. III D it appears that a picture where the  $(p_{1/2})^2$  and  $(s_{1/2})^2$  configurations have roughly equal weight is consistent with our calculations. To explain the large increase in the charge radius a large  $(s_{1/2})^2$  component is needed. The changes in the magnetic dipole moment and the electric quadrupole moment can only be explained by the  $(p_{1/2})^2$  component, which includes a certain degree of core polarization.

The *ab initio* Green's function Monte Carlo calculations with two- and three-body forces provide overall a good description of the binding energies and the electromagnetic properties of the lithium isotopes up to  ${}^9\text{Li}$  [25,70]. The values listed in Table V include statistical error bars. Unfortunately no results for  ${}^{11}\text{Li}$  are available. The GFMC calculations predict the right trend in the charge radii and the radii of

TABLE V. Ground state properties observed by laser spectroscopy (charge radius  $R_c$ , magnetic dipole moment  $\mu$ , and spectroscopic electric quadrupole moment  $Q_s$ ) compared to the results of nuclear model calculations. Experimental dipole and quadrupole moments of Li isotopes are taken from [6], results on  $^{11}\text{Li}$  are from [7]. Point-proton radii from theory are converted into charge radii according to Eq. (13) using the CODATA value for the proton radius [58] but neglecting the spin-orbit contribution. Using the proton radius from [64] will shift these values by about  $-0.012$  fm. Nuclear models are GFMC: Green's function Monte Carlo (AV18/IL3), FMD: fermionic molecular dynamics, NCSM: no-core shell model, TOSM: tensor-optimized shell model, SVMC: stochastic variational multicluster model (see text), 3BM: three-body wave function fitted to experimental data [36]. Masses, binding energies and the  $^{11}\text{Li}$  two-neutron separation energy  $S_{2n}$  are discussed in the text.

	$^6\text{Li}$	$^7\text{Li}$	$^8\text{Li}$	$^9\text{Li}$	$^{11}\text{Li}$	Ref
Nuclear charge radii $R_c$ (fm)						
Exp.	2.59(4)	2.44(4)	2.34(5)	2.25(5)	2.48(4)	this work
FMD	2.52	2.41	2.36	2.26	–	this work
GFMC <sup>a</sup>	2.58(1)	2.46(1)	2.25(1)	2.16(1)	–	[25,70]
NCSM(CDB2k)	2.40(6)	2.36(7)	2.31(8)	2.25(10)	2.26(13)	[27]
TOSM	–	–	–	2.23	2.44	[68]
SVMC <sup>a</sup>	–	2.41	2.32	2.23 <sup>b</sup> /2.25 <sup>c</sup>	2.53/2.26 <sup>d</sup>	[31,71]
3BM	–	–	–	–	2.466 <sup>e</sup>	[36]
Magnetic dipole moment $\mu$ ( $\mu_N$ )						
Exp.	0.822 047 3(6)	3.256 427(2)	1.653 560(18)	3.43678(6)	3.6712(3)	[6,7,72]
FMD	0.87	3.19	1.57	3.33	–	this work
GFMC	0.800(1) <sup>f</sup>	3.168(13) <sup>f</sup>	1.12(1)	2.54(2)	–	[49,70,73]
NCSM(CDB2k)	0.843(5)	3.01(2)	1.24(6)	2.89(2)	3.56(4)	[27]
TOSM	–	–	–	3.69	3.77	[68]
SVMC	–	3.15	1.17	3.43 <sup>b</sup> /3.40 <sup>c</sup>	3.23/3.21 <sup>d</sup>	[31,71]
3BM	–	–	–	–	3.671	[36]
Spectroscopic electric quadrupole moment $Q_s$ (mb)						
Exp.	–0.806(6)	–40.0(3)	+31.4(2)	–30.6(2)	(–)33.3(5)	[6,7,74]
FMD	–0.61	–39.3	+29.0	–28.7	–	this work
GFMC	–3.5(6)	–34(1)	+32(1)	–27(1)	–	[25,70]
NCSM(CDB2k)	–0.66(40)	–32.0(2.2)	+27.8(1.2)	–26.6(2.2)	–28.1(2.7)	[27]
TOSM	–	–	–	–26.5	–28	[68]
SVMC	–	–36.5	+22.3	–27.4 <sup>b</sup> /–33.7 <sup>c</sup>	–37.1/–35.2 <sup>d</sup>	[31,71]
3BM	–	–	–	–	–33.24	[36]
Mass $M$ (amu), binding energy $E_B$ (MeV)						
Exp. $M$ (amu)	6.015122794(16)	7.0160034256(45)	8.02248624(12)	9.02679020(21)	11.04372361(69)	[42,43,75]
Exp. $E_B$ (MeV)	31.99	39.25	41.28	45.34	45.71	[42,43,75]
Exp. $S_{2n}$ (MeV)	–	–	–	–	0.36915(65)	[42]
FMD $E_B$ (MeV)	31.20	38.38	40.13	43.86	–	this work
GFMC $E_B$ (MeV)	32.2(1)	39.3(2)	41.2(3)	46.7(5)	–	[49,70]
NCSM (CDB2k) $E_B$ (MeV)	29.07(41)	35.56(23)	35.82(22)	37.88(82)	37.72(45)	[27]
NCSM (INOY) $E_B$ (MeV)	32.33(19)	39.62(40)	41.27(51)	45.86(74)	42.50(95)	[27]
TOSM	–	–	–	45.3	$S_{2n} = 0.31$	[68]
SVMC	–	–	41.09 <sup>g</sup>	44.83 <sup>b,g</sup> /45.16 <sup>c,h</sup>	$S_{2n} = 0.34/0.12d$	[31,71]

<sup>a</sup>Point-proton radii converted to charge radii according to Eq. (13) using the CODATA value for the proton radius [58] but neglecting the spin-orbit contribution.

<sup>b</sup>Full calculation in SVMC, Minnesota potential ( $u = 1.0$ ), Table III [71].

<sup>c</sup>Truncated model space in SVMC, Minnesota potential ( $u = 1.0285$ ), Table III [71]. This is the basis for  $^{11}\text{Li}$  calculations in SVMC.

<sup>d</sup>Result of a frozen-core calculation.

<sup>e</sup>Based on  $R_{c-2n} = 5.55$  fm (Table 5 in [36]) and the experimental value for  $^9\text{Li}$  (this work).

<sup>f</sup>Including contributions from meson exchange currents in AV18/IL2 [73].

<sup>g</sup>Calculated using the experimental value of 36.778 MeV for the  $\alpha + t$  threshold.

<sup>h</sup>Calculated using the experimental value of 39.25 MeV for the  $^9\text{Li} + 2n$  threshold.

$^{6,7}\text{Li}$  are in excellent agreement with experiment, however the radii of  $^{8,9}\text{Li}$  are both about 3% too small. For the calculation of the magnetic moments of  $^{6,7}\text{Li}$  the contributions of meson-exchange currents have been included [73]: They add about 10% to the magnetic moment of  $^7\text{Li}$ , while in  $^6\text{Li}$  the contribution is less than 2% and negative. The results for  $^{6,7}\text{Li}$

agree very well with the experimental data, those for  $^{8,9}\text{Li}$  (as all other models without including meson exchange currents) underestimate them. The quadrupole moments from GFMC are all somewhat too small, especially in the case of  $^7\text{Li}$ .

The *ab initio* no-core shell model (NCSM) [26,76] is represented in Figs. 5 and 6 by calculations with the

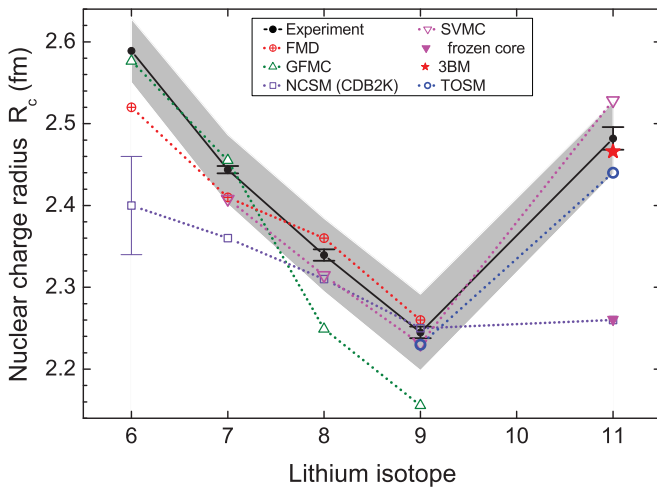


FIG. 5. (Color online) Charge radii  $R_c$  of the lithium isotopes as extracted from the isotope shift measurements ( $\bullet$ ). Error bars are based on the isotope shift uncertainty only. The additional systematic uncertainty caused by the reference charge radius uncertainty is indicated by the gray area (see text). Nuclear charge radii obtained from nuclear models are also shown: GFMC: Green's function Monte Carlo calculations [25,70], SVMC: stochastic variational multicluster model [31,71] (full triangles: assuming a frozen  ${}^9\text{Li}$  core), FMD: fermionic molecular dynamics (this work), NCSM: no-core shell model with Bonn CD2K interaction [27], TOSM: tensor-optimized shell model [68], and 3BM: three-body model (for  ${}^{11}\text{Li}$  only) [36]. A typical uncertainty for the NCSM calculations is indicated for  ${}^6\text{Li}$ . The other isotopes have similar uncertainties.

two-nucleon CD-Bonn 2000 (CDB2k) interaction as reported in [27]. While the INOY interaction gives binding energies closer to the experimental values (compare Table V), the CDB2k results for the electromagnetic observables show overall a better agreement with the experimental values. In the available model spaces the NCSM results are not yet converged and have to be extrapolated. The uncertainties due to extrapolation and the dependence on the oscillator constant are given in Table V for all isotopes but indicated in Fig. 5 only for  ${}^6\text{Li}$ , as a representative for all isotopes. The NCSM results show declining values for the charge radii going from  ${}^6\text{Li}$  to  ${}^9\text{Li}$ . While the values for  ${}^{6,7}\text{Li}$  are significantly too small, the charge radii for  ${}^8\text{Li}$  and  ${}^9\text{Li}$  are in good agreement with experiment. The magnetic dipole moments up to  ${}^9\text{Li}$  are, with the exception of  ${}^6\text{Li}$ , somewhat too small compared to experiment. A similar behavior is found for the electric quadrupole moments. The calculated charge radius of  ${}^{11}\text{Li}$  is almost unchanged from the  ${}^9\text{Li}$  value. The magnetic moment and the quadrupole moment on the other hand increase in  ${}^{11}\text{Li}$  compared to  ${}^9\text{Li}$ . These results seem to indicate that the NCSM  ${}^{11}\text{Li}$  wave function corresponds to an almost pure  $(p_{1/2})^2$  configuration. Within the harmonic oscillator basis it is extremely difficult to describe the loosely bound halo neutrons in the  $(s_{1/2})^2$  configuration of  ${}^{11}\text{Li}$ . In the future it might be possible to get a fully microscopic *ab initio* calculation for  ${}^{11}\text{Li}$  by combining the NCSM with the cluster model [77,78]. Similar results as with the CDB2k and INOY interactions were

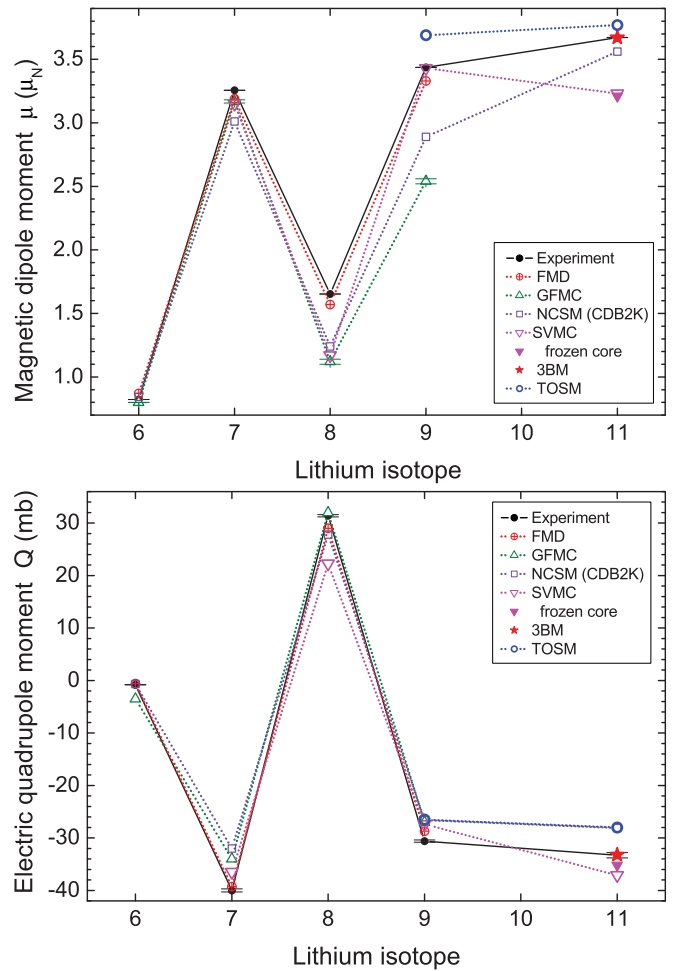


FIG. 6. (Color online) Magnetic dipole moment  $\mu$  (upper graph) and spectroscopic electric quadrupole moment  $Q_s$  (lower graph) of the lithium isotopes as determined by laser spectroscopic measurements ( $\bullet$ ) and calculated by nuclear models: GFMC: Green's function Monte Carlo calculations [49,70,73], SVMC: stochastic variational multicluster model [31,71] (full triangles: assuming a frozen  ${}^9\text{Li}$  core), FMD: fermionic molecular dynamics (this work), NCSM: no-core shell model with Bonn CD2K interaction [27], TOSM: tensor-optimized shell model [68], and 3BM: three-body model [36]. Experimental error bars are indicated but always smaller than the symbols. All values and references are listed in Table V.

obtained in NCSM calculations for  ${}^{6,7}\text{Li}$  using the UCOM force [57].

While the cluster structure of light nuclei emerges naturally in the FMD calculations, it is explicitly introduced in cluster models. In the stochastic variational microscopic multicluster model (SVMC) the lithium isotopes  ${}^{7-9}\text{Li}$  are described using microscopic wave functions built from  ${}^4\text{He}$  and  ${}^3\text{H}$  clusters and individual neutrons [31]. The SVMC tries to solve for the relative motion of the clusters and the neutrons using a stochastic variational method. The central Minnesota interaction with the exchange parameter  $u = 1.0$  together with a spin-orbit force adjusted to reproduce the splitting between the  $3/2^-$  and  $1/2^-$  states in  ${}^7\text{Li}$  was used. Based on these results a calculation for  ${}^{11}\text{Li}$  was performed in a

${}^9\text{Li}$  plus two-neutron model space. To make the calculation feasible a restricted set of  ${}^9\text{Li}$  configurations had to be employed in this calculation. The exchange parameter of the Minnesota interaction was changed slightly ( $u = 1.0285$ ) to make  ${}^{10}\text{Li}$  unbound. The obtained binding energies for  ${}^9\text{Li}$  and  ${}^{11}\text{Li}$  are close to experiment. The SVMC results show excellent agreement for the nuclear charge radii of  ${}^{7-9}\text{Li}$  and a reasonable agreement for magnetic and quadrupole moments. The relatively large deviation in  ${}^8\text{Li}$  might be traced back to the simplified interaction which does not contain a tensor component. For  ${}^{11}\text{Li}$  there are results with a frozen  ${}^9\text{Li}$  core in its ground state and a full calculation where the core can be polarized. The charge radius of  ${}^{11}\text{Li}$  in the full calculation with the polarized core agrees very well with the experimental result, whereas the calculation with the frozen  ${}^9\text{Li}$  core gives a charge radius that is too small and very close to that of the core. The quadrupole moment of  ${}^{11}\text{Li}$  is somewhat too large but the difference to the value for  ${}^9\text{Li}$  in the restricted model space appears reasonable. On the other hand the quadrupole moment of  ${}^9\text{Li}$  in the full calculation [31] differs quite strongly from the result in the restricted model space [71]. The magnetic moments of  ${}^{11}\text{Li}$  in both calculations are smaller than that of  ${}^9\text{Li}$  which is in disagreement with experiment and all other calculations. In summary the SVMC results seem to indicate that the charge radius in  ${}^{11}\text{Li}$  increases mainly due to core polarization.

### B. Three-body models and the center-of-mass motion in ${}^{11}\text{Li}$

Whereas the description of halo nuclei is very demanding in microscopic approaches these weakly bound systems are good candidates for potential models. The two-neutron separation energy in  ${}^{11}\text{Li}$  of 369.15(65) keV [42] is much smaller than the energy of the first excited state in  ${}^9\text{Li}$  (a  $1/2^-$  state at 2.69 MeV). It is therefore expected that core polarization effects are small and a three-body model for  ${}^{11}\text{Li}$  is expected to work well. To describe the three-body system an effective core-nucleon interaction is needed, antisymmetrization is sometimes included in an effective way by employing a repulsive Pauli potential. The parameters of the core-neutron interaction are adjusted to reproduce the  ${}^{10}\text{Li}$  resonances. To reproduce the  ${}^{11}\text{Li}$  binding energy typically an additional three-body force is added. However, the parameters and results of these models show a large variation. A particular example is the amount of  $s_{1/2}^2$  contribution to the ground state of  ${}^{11}\text{Li}$ , which reaches from 23% [62] up to 80% [79].

The tensor-optimized shell model (TOSM) [32] is essentially such a three-body model that keeps a microscopic picture of the core and allows for core excitations. It was developed in particular to study the role of tensor correlations, and provides only results for  ${}^{9,11}\text{Li}$  [32,67–69]. Starting from a microscopic picture of the  ${}^9\text{Li}$  core, the role of tensor and pairing correlations in  ${}^{11}\text{Li}$  are investigated in a three-body model to explain the large  $(s_{1/2})^2$  contribution to the  ${}^{11}\text{Li}$  ground state, which is a precondition for the halo formation. To describe the  ${}^9\text{Li}$  core an effective interaction based on a  $G$ -matrix interaction is used. The interaction is modified to reproduce the experimental binding energy and the radius of

${}^9\text{Li}$ . The core-neutron interaction is derived by folding the  ${}^9\text{Li}$  wave functions with the MHN force, another effective interaction. Antisymmetry is taken into account by adding a Pauli potential. Parameters of the MHN force are adjusted to reproduce the two-neutron separation energy within the three-body model. It is obvious from Figs. 5 and 6 that the TOSM reproduces the charge radius quite well and the electromagnetic moments with reasonable accuracy.

Recently, Shulgina, Jonson, and Zhukov constructed a three-body wave function of  ${}^{11}\text{Li}$  not by solving the three-body Schrödinger equation dynamically but by fitting the parameters of the three-body wave function directly to reproduce well determined experimental data [36]. Whereas magnetic moment and quadrupole moment were fitted directly, the charge radius was constrained to a range given by the direct charge radius measurements and the slightly smaller value deduced from the electric dipole strength. The value for the charge radius from the fit agrees very well with experiment.

To gain deeper insight into the  ${}^{11}\text{Li}$  Borromean system, the influence of the center-of-mass (c.m.) motion of the  ${}^9\text{Li}$  core must be separated from the  ${}^9\text{Li}$  core polarization. While the first is a pure geometrical consequence of the three-body system, the latter allows conclusions about the interaction between the halo-neutrons and the core. In a “pure” three-body model with a frozen core, a change of the nuclear charge radius can only occur from c.m. motion. The result of Ref. [36] shows that a pure three-body wave function of  ${}^{11}\text{Li}$  can in principle account for all experimentally known properties of the halo isotope consistently. However, contributions of core excitation cannot be excluded by this fit.

The effect of the c.m. motion on the nuclear charge radius can be most easily formulated for a nucleus consisting of point-like nucleons as

$$\langle r_{\text{pp}}^2(Z, A) \rangle = \langle r_{\text{pp}}^2(Z, A - 2) \rangle + \left(\frac{2}{A}\right)^2 \langle r_{\text{c-2n}}^2 \rangle \quad (16)$$

with the distance between the center of mass of the two halo neutrons and of the core ( $r_{\text{c-2n}}^2$ ). Equation (13) can be used to calculate  $\langle r_{\text{c}}^2 \rangle$  from the ms radius  $\langle r_{\text{pp}}^2 \rangle$  of the distribution of point-like protons. The difference in the mean square nuclear charge radii that is observed in the laser spectroscopic measurement is obtained by combining Eqs. (16) and (13)

$$\begin{aligned} \delta \langle r_{\text{c}}^2 \rangle^{9,11} &= \langle r_{\text{c}}^2({}^{11}\text{Li}) \rangle - \langle r_{\text{c}}^2({}^9\text{Li}) \rangle \\ &= \left(\frac{2}{11}\right)^2 \langle r_{\text{c-2n}}^2 \rangle + \frac{2}{3} R_n^2 + \langle r_{\text{c}}^2 \rangle_{\text{so}}^{(2n)\text{-halo}}. \end{aligned} \quad (17)$$

The proton radius and the Darwin-Foldy correction drop out completely in  $\delta \langle r_{\text{c}}^2 \rangle$ . In lowest order, the change in  $\langle r_{\text{c}}^2 \rangle$  is solely caused by the c.m. motion, but there are contributions by the mean square charge radius of the halo neutrons ( $\frac{2}{3} R_n^2 = -0.078 \text{ fm}^2$ ) and the spin-orbit charge density of the halo. If there is appreciable amount of core excitation it has to be considered with an additional term  $\langle r_{\text{c}}^2 \rangle_{\text{core-excitation}}$  in Eq. (17).

The size of the SO contributions in the TOSM model was obtained for  ${}^{9,11}\text{Li}$  using Eq. (14) and the corresponding wave-function composition [69] and the results are included in Table IV. The tensor and pairing correlations lead to a strong

admixture of almost 50% of the  $(s_{1/2})^2$  state to the  $^{11}\text{Li}$  ground state. The other major contributions have the two neutrons in the  $(p_{1/2})^2$ ,  $(p_{3/2})^2$ ,  $(d_{5/2})^2$ , and  $(d_{3/2})^2$  configurations with relative contributions of 42.7%, 2.5%, 4.1%, and 1.9%, respectively. The resulting spin-orbit term caused exclusively by the halo neutrons is  $\langle r_c^2 \rangle_{\text{so}}^{2n-\text{halo}} = 0.052 \text{ fm}^2$  and largely cancels the  $-0.071 \text{ fm}^2$  contribution of the core. The (negative) contribution of the neutrons in the  $^9\text{Li}$  core in  $^{11}\text{Li}$  is about 7% larger than for the free  $^9\text{Li}$  nucleus because the probability for  $2p-2h$  excitations, which give a positive contribution, is significantly reduced. This is a direct sign of the influence of the halo neutrons onto the core and the fact that the total neutron contribution to the spin-orbit term in  $^{11}\text{Li}$  is not zero, is a clear indication for the  $N = 8$  shell breaking.

The two-neutron core distance  $R_{c-2n} = 5.01(32) \text{ fm}$  obtained from Coulomb dissociation experiments [44] can be used to calculate a contribution of  $\delta \langle r_c^2 \rangle_{\text{CD}}^{9,11} = 0.78 \text{ fm}^2$  ( $\sim 70\%$  of the laser spectroscopic value) arising from c.m. motion. Reevaluation of the experimental data in [62], where the long high-energy tail of the transition strength was treated differently than in [44], resulted in  $\delta \langle r_c^2 \rangle_{\text{CD}}^{9,11} = 0.88(11) \text{ fm}^2$ . This value includes also a spin-orbit contribution of  $0.062 \text{ fm}^2$ . The difference

$$\begin{aligned} \delta \langle r_c^2 \rangle_{\text{Exp}}^{9,11} - \delta \langle r_c^2 \rangle_{\text{CD}} &= 1.12(8) - 0.88(11) \\ &= 0.24(14) \text{ fm}^2 \end{aligned} \quad (18)$$

can be attributed to core excitation. Backwards, we can calculate  $R_{c-2n}$  required to produce the measured  $\delta \langle r_c^2 \rangle_{\text{Exp}}^{9,11}$  in the absence of core excitation and assuming  $\langle r_c^2 \rangle_{\text{so}}^{(2n-\text{halo})} = 0.05 \text{ fm}^2$  and obtain  $R_{c-2n} = 5.89(3) \text{ fm}$ .

In the TOSM microscopic model the authors determine the  $R_{c-2n}$  distance to be  $5.69 \text{ fm}$ . Therefore, the change in the mean-square charge radius between  $^9\text{Li}$  and  $^{11}\text{Li}$  arising from the c.m. motion is  $0.992 \text{ fm}^2$ , which increases to  $1.044 \text{ fm}^2$  if the spin-orbit contribution of the halo neutrons is included according to the wave function from [68] (see Table IV). This is already close to the experimental value. Moreover, the full TOSM calculation delivered

$$\delta \langle r_c^2 \rangle_{\text{TOSM}}^{9,11} = 2.44^2 - 2.23^2 = 0.981 \text{ fm}^2 \quad (19)$$

indicating a very small amount of core excitation.

Pure three-body models abandon from the beginning any core excitation and construct  $^{11}\text{Li}$  wave functions based on an inert  $^9\text{Li}$  core and two neutrons. For the wave function presented in [36] a separation of  $R_{c-2n} = 5.55 \text{ fm}$  is reported. Using this and the experimental value for the charge radius of  $^9\text{Li}$ ,  $R_c(^{11}\text{Li}) = 2.466 \text{ fm}$  is obtained, as plotted in Fig. 5. The agreement with the experimental charge radius is excellent, which is not so surprising since the experimental values from laser spectroscopy and Coulomb dissociation were used as constraints in the fitting of the wave function. The magnitude of the halo neutron's spin-orbit term obtained with the three-body wave function from Table 4 in Ref. [36] and listed in Table IV, is very similar to that of the TOSM result. It changes the charge radius by about  $0.010 \text{ fm}$  and moves it even closer to the experimental value. The wave function also gives, by construction, excellent agreement for the nuclear magnetic moment and the quadrupole moment of the halo nucleus. This

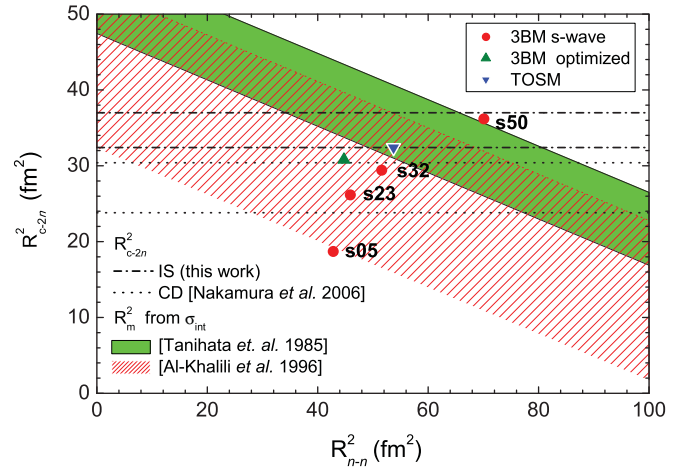


FIG. 7. (Color online) Constraints on the mean square core-2n distance  $R_{c-2n}^2$  and the mean square neutron-neutron distance  $R_{n-n}^2$  in a three-body model of  $^{11}\text{Li}$  obtained from the laser spectroscopic isotope shift measurements (this work) (IS, dash-dotted lines), the Coulomb dissociation experiment [44] (CD, dotted lines), and the matter radius ( $R_m$ ) according to Eq. (20) based on interaction cross section measurements  $\sigma_{\text{int}}$  [80] analyzed either in [80] (hatched) or [81] (shaded). The results obtained in various three-body model calculations (3BM) and the tensor-optimized shell model (TOSM) are also indicated;  $\bullet$ : 3BM with 5–50%  $s$ -wave contributions according to Table II in [62],  $\blacktriangle$ : 3BM optimized to reproduce all experimental data available for  $^{11}\text{Li}$  [36],  $\blacktriangledown$ : TOSM calculations [68]. The spin-orbit contribution was neglected in all cases.

demonstrates that a three-body wave function can in principle fully account for the small difference between the  $^9\text{Li}$  and  $^{11}\text{Li}$  nuclear spectroscopic quadrupole moments by including components with  $J_{\text{Halo}} > 0$  to the halo wave function.

It was pointed out by Esbensen and coworkers [62] that the difference in Eq. (18) can be combined with information on the matter radius to get a better picture of the  $^{11}\text{Li}$  geometry. While the  $B(E1)$  strength distribution and the charge radius are only sensitive to  $\langle r_{c-2n}^2 \rangle$ , the matter radius depends also on the mean square distance between the halo neutrons  $\langle r_{n-n}^2 \rangle$  according to [62]

$$\begin{aligned} \langle r_m^2(Z, A) \rangle &= \frac{A-2}{A} \langle r_m^2(Z, A-2) \rangle \\ &+ \frac{2(A-2)}{A^2} \langle r_{c-2n}^2 \rangle + \frac{1}{2A} \langle r_{n-n}^2 \rangle. \end{aligned} \quad (20)$$

This is shown in Fig. 7, where  $\langle r_{c-2n}^2 \rangle$  is plotted against  $\langle r_{n-n}^2 \rangle$ . The hatched area indicates the range of allowed radii parameters based on the nuclear matter radii from the Tanihata measurements [80], the dotted and the dash-dotted lines represent the  $1-\sigma$  range for  $\langle r_{c-2n}^2 \rangle$  obtained from Coulomb dissociation and the charge radius measurements, respectively. In Ref. [62] it is argued that the Coulomb dissociation result and the matter radii favor a 23%  $s$ -orbital contribution (s23 model), while the difference to the charge radius result is ascribed to core excitation.

However, this conclusion depends strongly on the  $^{11}\text{Li}$  matter radius. The value reported in [80] became questionable

because the correlation of the halo neutrons was not considered in the Glauber-type calculations used to extract the matter radius. A reanalysis performed in Ref. [81] resulted in a considerably larger matter radius of  $R_m = 3.55(10)$  fm. This value is also in accordance with  $R_m = 3.71(20)$  fm obtained from medium-energy elastic proton scattering in inverse kinematics performed more recently at GSI [82]. The shaded area shows the allowed radii parameters according to the value from [81]. Now the conclusion drawn in [62] is not as obvious anymore and even the 50%  $(s_{1/2})^2$  calculation is at the edge of the band while the s23 model is far outside.

The TOSM calculation, which is not a pure three-body model calculation, as well as the three-body model by Shulgina and coworkers [36] indicate a clearly larger  $(s_{1/2})^2$  probability than 23%, reducing the amount of core polarization. In summary, it must be concluded that an unambiguous separation of core-excitation and c.m. motion is still not possible.

## V. CONCLUSION

We have summarized the results of nuclear charge radius measurements on the complete chain of lithium isotopes and extracted absolute charge radii based on a reevaluation of the world data on elastic electron scattering of  ${}^6\text{Li}$ . Furthermore, new calculations for the ground state properties of  ${}^{6-9}\text{Li}$  using fermionic molecular dynamics were presented and the contribution of the spin-orbit term to the nuclear charge radius was estimated for all isotopes based on realistic wave functions. Results for charge radii and the electromagnetic moments

were compared to the predictions of a variety of nuclear structure models. While many microscopic models are able to reproduce the trend of nuclear charge radii from  ${}^{6-9}\text{Li}$  the description of  ${}^{11}\text{Li}$  presents a tough challenge for microscopic models. The stochastic variational multicluster model provides a charge radius close to experiment but the comparison is less convincing for the magnetic moment and the quadrupole moment. Surprisingly calculations with a frozen  ${}^9\text{Li}$  core give a much smaller  ${}^{11}\text{Li}$  charge radius. Three-body calculations with an underlying microscopic picture in the tensor-optimized shell model also agree well with the experimental  ${}^{11}\text{Li}$  charge radius. However parameters of the effective interactions had to be adjusted to reproduce  ${}^9\text{Li}$  and  ${}^{11}\text{Li}$  properties. A three-body wave function fitted to experimental observables is also able to reproduce all  ${}^{11}\text{Li}$  properties consistently. An unambiguous separation between the center-of-mass motion and core excitation using the charge radius, the matter radius and information from Coulomb dissociation is unfortunately still not possible.

## ACKNOWLEDGMENTS

This work was supported by BMBF (contract no. 06MZ9178I) and by the Helmholtz Association of German Research Centres (contract no. VH-NG 148). We thank J. Kluge for many discussions and for supporting the project for many years, T. Myo for providing unpublished details of his wave functions, and B. Jonson, R. Neugart, and H. Feldmeier for valuable discussions.

- 
- [1] W. E. Otten, *Nuclear Radii and Moments of Unstable Isotopes*, Treatise of Heavy Ion Physics, Vol. 8 (Plenum Press, New York, 1987).
  - [2] H.-J. Kluge and W. Nörtershäuser, *Spectrochim. Acta, Part B* **58**, 1031 (2003).
  - [3] E. Arnold *et al.*, *Phys. Lett. B* **197**, 311 (1987).
  - [4] E. Arnold *et al.*, *Phys. Lett. B* **281**, 16 (1992).
  - [5] W. Geithner *et al.*, *Hyperfine Interact.* **127**, 117 (2000).
  - [6] D. Borremans *et al.*, *Phys. Rev. C* **72**, 044309 (2005).
  - [7] R. Neugart *et al.*, *Phys. Rev. Lett.* **101**, 132502 (2008).
  - [8] J. Billowes and P. Campbell, *J. Phys. G* **21**, 707 (1995).
  - [9] R. Neugart, *Europ. Phys. J. A* **15**, 35 (2002).
  - [10] Z.-C. Yan and G. W. F. Drake, *Phys. Rev. A* **61**, 022504 (2000).
  - [11] Z.-C. Yan and G. W. F. Drake, *Phys. Rev. Lett.* **91**, 113004 (2003).
  - [12] M. Puchalski, A. M. Moro, and K. Pachucki, *Phys. Rev. Lett.* **97**, 133001 (2006).
  - [13] Z. C. Yan, W. Nörtershäuser, and G. W. F. Drake, *Phys. Rev. Lett.* **100**, 243002 (2008).
  - [14] M. Puchalski and K. Pachucki, *Phys. Rev. A* **79**, 032510 (2009).
  - [15] G. Ewald *et al.*, *Phys. Rev. Lett.* **93**, 113002 (2004).
  - [16] G. Ewald *et al.*, *Phys. Rev. Lett.* **94**, 039901(E) (2005).
  - [17] L.-B. Wang *et al.*, *Phys. Rev. Lett.* **93**, 142501 (2004).
  - [18] R. Sánchez *et al.*, *Phys. Rev. Lett.* **96**, 033002 (2006).
  - [19] P. Müller *et al.*, *Phys. Rev. Lett.* **99**, 252501 (2007).
  - [20] W. Nörtershäuser *et al.*, *Phys. Rev. Lett.* **102**, 062503 (2009).
  - [21] W. Nörtershäuser *et al.*, *Phys. Rev. A* **83**, 012516 (2011).
  - [22] R. Engfer *et al.*, *At. Data Nucl. Data Tables* **14**, 509 (1973).
  - [23] S. Schaller, *Z. Phys. C* **56**, 48 (1992).
  - [24] J. Carlson, *Phys. Rev. C* **36**, 2026 (1987).
  - [25] S. C. Pieper, and R. B. Wiringa, *Annu. Rev. Nucl. Part. Sci.* **51**, 53 (2001).
  - [26] P. Navrátil and B. R. Barrett, *Phys. Rev. C* **57**, 3119 (1998).
  - [27] C. Forssen, E. Caurier, and P. Navratil, *Phys. Rev. C* **79**, 021303(R) (2009).
  - [28] P. Navrátil, S. Quaglioni, I. Stetcu, and B. R. Barrett, *J. Phys. G* **36**, 083101 (2009).
  - [29] E. Epelbaum, H. Krebs, D. Lee, and Ulf.-G. Meißner, *Phys. Rev. Lett.* **104**, 142501 (2010).
  - [30] T. Neff and H. Feldmeier, *Eur. Phys. J. Special Topics* **156**, 69 (2008).
  - [31] K. Varga, Y. Suzuki, and I. Tanihata, *Phys. Rev. C* **52**, 3013 (1995).
  - [32] T. Myo, K. Kato, and K. Ikeda, *Prog. Theor. Phys.* **113**, 763 (2005).
  - [33] L. R. Suelzle, M. R. Yearian, and H. Crannell, *Phys. Rev.* **162**, 992 (1967).
  - [34] F. A. Bumiller, F. R. Buskirk, J. N. Dyer, and W. A. Monson, *Phys. Rev. C* **5**, 391 (1972).
  - [35] G. C. Li, I. Sick, R. R. Whitney, and M. R. Yearian, *Nucl. Phys. A* **162**, 583 (1971).
  - [36] N. B. Shulgina, B. Jonson, and M. V. Zhukov, *Nucl. Phys. A* **825**, 175 (2009).
  - [37] M. Puchalski and K. Pachucki, *Phys. Rev. A* **78**, 052511 (2008).
  - [38] G. Audi and A. H. Wapstra, *Nucl. Phys. A* **595**, 409 (1995).

- [39] Z.-C. Yan and G. W. F. Drake, *Phys. Rev. A* **66**, 042504 (2002).
- [40] C. Bachelet *et al.*, *Eur. Phys. J. A* **25**, 31 (2005).
- [41] C. Bachelet *et al.*, *Phys. Rev. Lett.* **100**, 182501 (2008).
- [42] M. Smith, M. Brodeur, T. Brunner, S. Effenauer, A. Lapierre, R. Ringle, V. L. Ryjkov, F. Ames, P. Bricault, G. W. F. Drake, P. Delheij, D. Lunney, F. Sarazin, and J. Dilling, *Phys. Rev. Lett.* **101**, 202501 (2008).
- [43] G. Audi, A. H. Wapstra, and C. Thibault, *Nucl. Phys. A* **729**, 337 (2003).
- [44] T. Nakamura *et al.*, *Phys. Rev. Lett.* **96**, 252502 (2006).
- [45] T. Janssens, R. Hofstadter, E. B. Hughes, and M. R. Yearian, *Phys. Rev.* **142**, 922 (1966).
- [46] H. Bentz, *Z. Phys.* **243**, 138 (1971).
- [47] J. Arrington and I. Sick, *Phys. Rev. C* **70**, 028203 (2004).
- [48] I. Sick, *Nucl. Phys. A* **218**, 509 (1974).
- [49] S. C. Pieper, V. R. Pandharipande, R. B. Wiringa, and J. Carlson, *Phys. Rev. C* **64**, 014001 (2001).
- [50] R. Wiringa (private communication).
- [51] M. Chernykh, H. Feldmeier, T. Neff, P. von Neumann-Cosel, and A. Richter, *Phys. Rev. Lett.* **98**, 032501 (2007).
- [52] M. Žáková *et al.*, *J. Phys. G: Nucl. Part. Phys.* **37**, 055107 (2010).
- [53] W. Geithner *et al.*, *Phys. Rev. Lett.* **101**, 252502 (2008).
- [54] T. Neff, *Phys. Rev. Lett.* **106**, 042502 (2011).
- [55] H. Feldmeier, T. Neff, R. Roth, and J. Schnack, *Nucl. Phys. A* **632**, 61 (1998).
- [56] T. Neff and H. Feldmeier, *Nucl. Phys. A* **713**, 311 (2003).
- [57] R. Roth, T. Neff, and H. Feldmeier, *Prog. Part. Nucl. Phys.* **65**, 50 (2010).
- [58] P. J. Mohr, B. N. Taylor, and D. B. Newell, *Rev. Mod. Phys.* **80**, 633 (2008).
- [59] S. Kopecky, J. A. Harvey, N. W. Hill, M. Krenn, M. Pernicka, P. Riehs, and S. Steiner, *Phys. Rev. C* **56**, 2229 (1997).
- [60] J. L. Friar, J. Martorell, and D. W. L. Sprung, *Phys. Rev. A* **56**, 4579 (1997).
- [61] J. L. Friar and J. W. Negele, *Adv. Nucl. Phys.* **8**, 219 (1975).
- [62] H. Esbensen, K. Hagino, P. Mueller, and H. Sagawa, *Phys. Rev. C* **76**, 024302 (2007).
- [63] A. Ong, J. C. Berengut, and V. V. Flambaum, *Phys. Rev. C* **82**, 014320 (2010).
- [64] R. Pohl *et al.*, *Nature (London)* **466**, 213 (2010).
- [65] I. Sick, *Phys. Lett. B* **576**, 62 (2003).
- [66] P. G. Blunden and I. Sick, *Phys. Rev. C* **72**, 057601 (2005).
- [67] T. Myo, K. Kato, H. Toki, and K. Ikeda, *Phys. Rev. C* **76**, 024305 (2007).
- [68] T. Myo, Y. Kikuchi, K. Kato, H. Toki, and K. Ikeda, *Prog. Theor. Phys.* **119**, 561 (2008).
- [69] Takayuki Myo (private communication).
- [70] S. C. Pieper, K. Varga, and R. B. Wiringa, *Phys. Rev. C* **66**, 044310 (2002).
- [71] K. Varga, Y. Suzuki, and R. G. Lovas, *Phys. Rev. C* **66**, 041302(R) (2002).
- [72] P. Raghavan, *At. Data Nucl. Data Tables* **42**, 189 (1989).
- [73] L. E. Marcucci, M. Pervin, S. C. Pieper, R. Schiavilla, and R. B. Wiringa, *Phys. Rev. C* **78**, 065501 (2008).
- [74] P. Pyykkö, *Mol. Phys.* **99**, 1617 (2001).
- [75] S. Nagy, T. Fritioff, M. Suhonen, R. Schuch, K. Blaum, M. Bjorkhage, and I. Bergstrom, *Phys. Rev. Lett.* **96**, 163004 (2006).
- [76] P. Navrátil and W. E. Ormand, *Phys. Rev. C* **68**, 034305 (2003).
- [77] S. Quaglioni and P. Navrátil, *Phys. Rev. C* **79**, 044606 (2009).
- [78] P. Navrátil and S. Quaglioni, *Phys. Rev. C* **83**, 044609 (2011).
- [79] E. Garrido, D. V. Fedorov, and A. S. Jensen, *Phys. Rev. C* **58**, 2654 (1998).
- [80] I. Tanihata, H. Hamagaki, O. Hashimoto, Y. Shida, N. Yoshikawa, K. Sugimoto, O. Yamakawa, T. Kobayashi, and N. Takahashi, *Phys. Rev. Lett.* **55**, 2676 (1985).
- [81] J. S. Al Khalili and J. A. Tostevin, *Phys. Rev. Lett.* **76**, 3903 (1996).
- [82] A. V. Dobrovolsky *et al.*, *Nucl. Phys. A* **766**, 1 (2006).